Theory of the Dynamic Light Scattering Properties for Circular Semiflexible Chains in Solution

Kunitsugu Soda

Department of Physics, Faculty of Science, University of Tokyo, Hongo, Bunkyo-ku, Tokyo 113, Japan. *Received October 26, 1983*

ABSTRACT: Berg's theory of the thermal motion of a circular semiflexible chain is extended by including the effect of intramolecular hydrodynamic interaction. An expression for its dynamic structure factor, $S(\mathbf{K},t)$, is given. Several quantities characterizing dynamic light scattering (DLS) properties are evaluated numerically for parameter values corresponding to DNA. Results of the numerical calculation are as follows: (1) The normalized DLS correlation function, $C(t)$, deviates significantly from single-exponential form in the large-K region. When a single-exponential function with a constant base is fitted to calculated $C(t)$ in the range of t that $C(t)$ is larger than 0.01, the base fraction relative to the correlation amplitude takes a saturated value of about 2% in the large-K region. (2) The reciprocal correlation time of the scattered light shows a K dependence significantly different from that predicted from the theory for Rouse–Zimm chains. (3) The apparent diffusion coefficients reduced to the standard state of water at 25 °C are fairly insensitive to changes in chain length, chain stiffness, and the solution temperature.

I. Introduction

The dynamic light scattering (DLS) method has become a valuable method for investigating the thermal motion of chain polymers in solution. Considerable efforts to extract the relaxation times of internal modes from the shape analysis of measured photocount correlation functions have been made mainly on synthetic polymers. For DLS measurements in which a visible or UV laser is used as the light source, most synthetic polymers can be treated as flexible chains because they have a persistence length much shorter than the inverse of the scattering vector, $1/K$, where

$$K = \frac{4\pi n}{\lambda} \sin\left(\frac{\theta}{2}\right) \tag{1}$$

λ being the wavelength of light, n the refractive index of the solution, and θ the scattering angle. First, we will briefly review the works on flexible polymers for later discussion.

Most of the theoretical studies on the dynamic properties of flexible polymer chains have been made on the Rouse–Zimm (RZ) model. de Gennes and Dubois-Violette (DD)[1-3] were first to apply Zimm's theory[4] of RZ chains to DLS problems and gave an explicit formula for the dynamic structure factor, $S(\mathbf{K},t)$, of these chains. They obtained the following important conclusion with regard to the spectral line width, Γ_s, of light scattered from a solution of RZ chains: if the chain is long enough to satisfy the condition

$$KR \gg 1 \tag{2}$$

where R is the root-mean-square radius, (1) Γ_s is a function of only the viscosity, η, temperature, T, of solvent, and K and is independent of the values of molecular parameters, and (2) it is proportional to K^4 in the free-draining limit and to K^3 when the effect of hydrodynamic interaction is taken into account.

Using Zimm's theory, Pecora[5] gave an expression of the power spectrum, $P(\mathbf{K},\omega)$, for RZ chains in the form of a series expansion with respect to the mode number of internal motion. Especially, he investigated precisely the form of $P(\mathbf{K},\omega)$ at K where the contributions from the translational and the lowest internal modes are dominant. In spite of many efforts, application of Pecora's theory to DNA has yielded few definite results.[6,7]

Some years ago, Akcasu and Gurol[8] (see also Benmouna et al.[9,10]) found that the first cumulant, $\Gamma(\mathbf{K})$, of the dynamic structure factor for a chain can be obtained from its equilibrium properties without preaveraging the Oseen tensor. They showed also that $\Gamma(\mathbf{K})$ of Gaussian chains has the same exponent for the dependence on K as Γ_s in DD theory, where Γ_s is the half-width at half-maximum of the power spectrum.

Lin and Schurr[11] obtained a formula for $S(\mathbf{K},t)$, solving the Langevin equation of motion for the RZ model. They showed that the apparent diffusion coefficient yielded from fitting a single-exponential function to $S(\mathbf{K},t)$ approaches a constant for sufficiently large values of K. This means that the spectral line width is proportional to K^2 in the above saturation region of K. They proposed an algorithm to determine RZ model parameters from measured data and applied it to the analysis of data for calf thymus DNA.

There are many biopolymers whose equilibrium properties are well described by the wormlike chain model.[12] Native DNA, collagen, muscle actin filament, and filamentous virus are examples. These molecules have a persistence length comparable to the inverse of the scattering vector available in DLS experiments. In addition to a bending stiffness, real wormlike molecules have a finite torsional stiffness. Therefore, it is expected that their DLS properties are different from those of flexible chains. It is very interesting how the semiflexible character of a chain affects its DLS properties.

As to DNA, which is the main concern of the author, all the analyses of its DLS data have so far been made with the RZ model.[6,7,11,13-16] The applicability of the RZ model to DNA and the physical interpretation of the model parameters were discussed in detail by Schurr and co-workers in their recent works.[17,16] The RZ model has some disadvantages in its application to DNA: (1) As described above, the DLS method enables the observation of a DNA molecule with a spatial resolution of the order of the persistence length. On such a scale, the real chain is far different from the model. As long as we stick to the model, we cannot have a true picture of the local dynamic behavior of the chain. (2) Relations between molecular parameters and RZ model parameters, i.e., the root-mean-square distance between adjacent beads, b, the number of beads, N, and the friction coefficient of a bead, f, are not yet established. Accordingly, for example, we cannot correlate quantitatively changes in the model parameters with those in the structural parameters of the chain which are caused by changes in external conditions.

The theoretical study of the dynamic properties of wormlike chains is very poorly developed compared with

0024-9297/84/2217-2365$01.50/0

that of flexible polymers. The main cause for this is the mathematical difficulty originating from the nonlinear form of the equation of motion. Harris and Hearst[18] (HH) proposed a model for stiff chains and developed a dynamic theory of their model. Hearst et al.[19] extended the HH theory by including the effect of hydrodynamic interaction. It was pointed out[20] that the HH theory gives a result inconsistent with the static theory[21,22] of wormlike chains. Maeda and Fujime[23] presented a theory for evaluating the DLS properties of the HH chain. It has the following defects: (1) The relation between bending force constant and persistence length is inconsistent with the result of static theory,[21,22] and (2) as the effect of hydrodynamic interaction is not included, it is difficult to apply their theory to the quantitative analyses of measured data. Recently, the first cumulant of the dynamic structure factor at low scattering vectors was calculated and compared for several models of semiflexible chains by Schmidt and Stockmayer.[24]

Berg[20] developed a dynamic theory of continuous semiflexible chains starting from a model similar to the HH model. As described later, the Berg theory is not a theory of wormlike chains because his model introduces the longitudinal stiffness of chains in an incomplete way. It is based on several assumptions noted in section IV. It has, however, an advantage over the others in that it can give essentially the same results as the well-established static theory for most equilibrium properties of wormlike chains.[21,22] For this reason, Berg's theory is considered to be the most valuable for describing the thermal motion of circular semiflexible chains.

In this paper, we extend Berg's theory by including the effect of intramolecular hydrodynamic interaction, not of the discrete bead–spring model but of the wormlike chain model, and give an explicit formula for the dynamic structure factor. Using this formula, we evaluate numerically quantities related to DLS properties and compare them with the available data.

II. Theory

Langevin Equation of Motion. After Berg, we begin with a discrete model. Let us consider a circular chain composed of N beads and N massless rods of length b. Assuming that the bending elasticity of the chain is given by the potential energy

$$V = (\epsilon_0/2)\sum_{j=1}^{N}(\mathbf{r}_{j+1} - 2\mathbf{r}_j + \mathbf{r}_{j-1})^2 \tag{3}$$

we have the equation of motion in the free-draining case as

$$m\ddot{\mathbf{r}}_j + f\dot{\mathbf{r}}_j + \epsilon_0(\mathbf{r}_{j+2} - 4\mathbf{r}_{j+1} + 6\mathbf{r}_j - 4\mathbf{r}_{j-1} + \mathbf{r}_{j-2}) - \kappa_{j+1}(\mathbf{r}_{j+1} - \mathbf{r}_j) + \kappa_j(\mathbf{r}_j - \mathbf{r}_{j-1}) = \mathbf{f}_j \qquad (j = 1, ..., N) \tag{4}$$

In eq 3 and 4, $\mathbf{r}_j(t)$ is the position vector of bead j, $\mathbf{f}_j(t)$ is the thermal force exerted on bead j, and m and f are the mass and the friction coefficient of a bead. κ_j are the Lagrange multipliers originating under the constraints that the bond lengths are constant. Though each κ_j depends generally on time, Berg solved eq 4 by assuming that the κ_j are independent of j and t, i.e., putting

$$\kappa_j = \kappa_0 \qquad (j = 1, ..., N) \tag{5}$$

With this assumption, eq 4 becomes equivalent to the equation of motion of a chain with the potential energy

$$V = (\epsilon_0/2)\sum_{j=1}^{N}(\mathbf{r}_{j+1} - 2\mathbf{r}_j + \mathbf{r}_{j-1})^2 + (\kappa_0/2)\sum_{j=1}^{N}(\mathbf{r}_j - \mathbf{r}_{j-1})^2 \tag{6}$$

in place of the constraints of the constant bond length. Therefore, in a solution of eq 4 with the assumption of eq 5, the distance between adjacent beads must vary with time. In the following, we also make the assumption of eq 5. Denoting

$$\mathbf{R} = \begin{bmatrix} \mathbf{r}_1 \\ \cdot \\ \cdot \\ \cdot \\ \mathbf{r}_N \end{bmatrix} \quad \text{and} \quad \mathbf{F} = \begin{bmatrix} \mathbf{f}_1 \\ \cdot \\ \cdot \\ \cdot \\ \mathbf{f}_N \end{bmatrix} \tag{7}$$

we can express eq 4 as

$$m\ddot{\mathbf{R}} + f\dot{\mathbf{R}} + \mathbf{A}\mathbf{R} = \mathbf{F} \tag{8}$$

where $\mathbf{A}$ is an $N \times N$ matrix

$$\mathbf{A} = \epsilon_0 \begin{bmatrix} 6,-4, 1, 0,..., 0, 1,-4 \\ -4, 6,-4, 1, 0,..., 0, 1 \\ 1,-4, 6,-4, 1, 0,..., 0 \\ 0, 1,-4, 6,-4, 1, 0,... \\ ..., 0, 1,-4, 6,-4, 1, 0 \\ 0,..., 0, 1,-4, 6,-4, 1 \\ 1, 0,..., 0, 1,-4, 6,-4 \\ -4, 1, 0,..., 0, 1,-4, 6 \end{bmatrix} + \kappa_0 \begin{bmatrix} 2,-1, 0,..., 0,-1 \\ -1, 2,-1, 0,..., 0 \\ 0,-1, 2,-1, 0,... \\ ..., 0,-1, 2,-1, 0 \\ 0,..., 0,-1, 2,-1 \\ -1, 0,..., 0,-1, 2 \end{bmatrix} \tag{9}$$

Here, we will introduce the effect of hydrodynamic interactions into eq 8. The equation of motion of bead j now becomes

$$m\ddot{\mathbf{r}}_j + f(\dot{\mathbf{r}}_j - \mathbf{v}_j^*) + \sum_k A_{jk}\mathbf{r}_k = \mathbf{f}_j \tag{10}$$

where A_{jk} is the (j,k) component of the matrix $\mathbf{A}$. $\mathbf{v}_j^*$ is the fluid velocity at $\mathbf{r}_j$ that is generated by the motion of the beads other than j. According to the Oseen interaction formula, it is given by

$$\mathbf{v}_j^* = f\sum_{k(\neq j)} \mathcal{T}_{jk}(\dot{\mathbf{r}}_k - \mathbf{v}_k^*) \tag{11}$$

where

$$\mathcal{T}_{jk} = \frac{1}{8\pi\eta r_{jk}}\left(\mathbf{e} + \frac{\mathbf{r}_{jk}\mathbf{r}_{jk}}{r_{jk}^2}\right) \tag{12}$$

In eq 12, η is the viscosity of the solvent, $\mathbf{e}$ is the unit tensor, and $\mathbf{r}_{jk}$ is the vector directed from bead k to j. Preaveraging the Oseen tensor eq 12 and introducing an $N \times N$ matrix $\mathbf{T}$ with the (j,k) component

$$T_{jk} \equiv \frac{1}{6\pi\eta}\left\langle\frac{1}{r_{jk}}\right\rangle \tag{13}$$

we can express eq 10 and 11 as

$$m\ddot{\mathbf{R}} + f(\dot{\mathbf{R}} - \mathbf{V}^*) + \mathbf{A}\mathbf{R} = \mathbf{F} \tag{14}$$

and

$$\mathbf{V}^* = f\mathbf{T}(\dot{\mathbf{R}} - \mathbf{V}^*) \tag{15}$$

where $\mathbf{V}^*$ is a column vector composed of $\mathbf{v}_1^*, ..., \mathbf{v}_N^*$. Defining the hydrodynamic interaction matrix $\mathbf{H}$ by

$$\mathbf{H} \equiv \mathbf{I} + f\mathbf{T} \tag{16}$$

where $\mathbf{I}$ is an $N \times N$ unit matrix, we get from eq 15

$$\mathbf{V}^* = (\mathbf{I} - \mathbf{H}^{-1})\dot{\mathbf{R}} \tag{17}$$

Substitution of eq 17 into eq 14 yields

$$m\ddot{\mathbf{R}} + f\mathbf{H}^{-1}\dot{\mathbf{R}} + \mathbf{AR} = \mathbf{F} \tag{18}$$

Equation 18 is the Langevin equation of motion of the chain with hydrodynamic interactions and corresponds to eq 13 of Zimm's theory.[4] Equation 1 of Lin and Schurr[11] is different from eq 18 and their equation gave several unphysical results. Using correct equilibrium properties which are not deduced from their equation, they avoided the internal inconsistency.

The closed nature of the chain permits a Fourier expansion of $\mathbf{R}$ as

$$\mathbf{R} = \mathbf{UQ} \tag{19}$$

where $\mathbf{U}$ is an $N \times N$ unitary matrix with the (j,n) component

$$U_{jn} = \frac{1}{N^{1/2}} \exp\left(-i\frac{2\pi jn}{N}\right) \tag{20}$$

and

$$\mathbf{Q} = \begin{bmatrix} \mathbf{q}_1 \\ \cdot \\ \cdot \\ \cdot \\ \mathbf{q}_N \end{bmatrix} \tag{21}$$

From eq 19, $\mathbf{Q}$ is given by

$$\mathbf{Q} = \mathbf{U}^{-1}\mathbf{R} \tag{22}$$

where

$$(\mathbf{U}^{-1})_{nj} = \frac{1}{N^{1/2}} \exp\left(i\frac{2\pi nj}{N}\right) \tag{23}$$

The matrix $\mathbf{A}$ is diagonalized by $\mathbf{U}$ to yield

$$(\mathbf{U}^{-1}\mathbf{AU})_{mn} = b\lambda_n\delta_{mn} \tag{24}$$

where

$$\lambda_n = (1/b)\{16\epsilon_0 \sin^4 (n\pi/N) + 4\kappa_0 \sin^2 (n\pi/N)\} \tag{25}$$

As is easily seen, H_{jk} depends on j and k only in the form of $|j - k|$. That is, we can put

$$H_{jk} = H(|j - k|) = H(N - |j - k|) \tag{26}$$

The matrix $\mathbf{H}$ is diagonalized also by $\mathbf{U}$ to give

$$(\mathbf{U}^{-1}\mathbf{HU})_{mn} = \gamma_n\delta_{mn} \tag{27}$$

where

$$\gamma_n = \sum_{l=0}^{N-1} H(l) \cos\left(\frac{2\pi nl}{N}\right) \tag{28}$$

From eq 27, we have

$$(\mathbf{U}^{-1}\mathbf{H}^{-1}\mathbf{U})_{mn} = (1/\gamma_n)\delta_{mn} \tag{29}$$

Dividing both sides of eq 18 by b and operating $\mathbf{U}^{-1}$ from the left side, we have decoupled equations of the normal modes as

$$\rho\ddot{\mathbf{q}}_n + \zeta_n\dot{\mathbf{q}}_n + \lambda_n\mathbf{q}_n = \mathbf{h}_n \qquad (n = 0, 1, ..., N-1) \tag{30}$$

where

$$\rho \equiv m/b \tag{30a}$$

$$\zeta_n \equiv \zeta/\gamma_n \tag{30b}$$

$$\zeta \equiv f/b \tag{30c}$$

and

$$\mathbf{h}_n = \frac{1}{(Nb)^{1/2}} \sum_{j=1}^{N} \mathbf{f}_j \exp\left(i\frac{2\pi nj}{N}\right) \tag{30d}$$

As already done in eq 30, "0" instead of "N" is used in the following as the suffix to denote the Nth normal mode. It can be easily shown that putting either $n = 0$ or $n = N$ leads to the same results in the related formulas.

From the comparison of eq 30 with eq 12 of Berg,[20] the effect of hydrodynamic interactions can be seen to appear in the form that the friction coefficient of each mode depends on its mode number. Equation 30 for $n = 0$ with $\lambda_n = 0$ corresponds to the translational motion of the whole chain. Neglecting the inertial term for $n \neq 0$, we can easily obtain from eq 30

$$\langle \mathbf{q}_n(t)\cdot\mathbf{q}_n^*(0)\rangle = \langle|\mathbf{q}_n|^2\rangle \exp(-t/\tau_n) \tag{31}$$

and

$$\langle|\mathbf{q}_n(t) - \langle\mathbf{q}_n(t)\rangle|^2\rangle = \langle|\mathbf{q}_n|^2\rangle(1 - \exp(-2t/\tau_n)) \tag{32}$$

where τ_n is the relaxation time of the nth normal mode given by

$$\tau_n = \zeta_n/\lambda_n \tag{33}$$

In the original model of beads and rods, the chain has $2N$ degrees of freedom, while it has $3N$ normal modes as seen from eq 30. Here, the equipartition of the thermal energy, $2NkT$, to the $3N$ normal modes is assumed as done by Berg, which leads to the relation

$$\langle|\mathbf{q}_n|^2\rangle = \frac{N - (3/2)}{N - 1}\frac{2kT}{b\lambda_n} \underset{N\to\infty}{\rightarrow} \frac{2kT}{b\lambda_n} \tag{34}$$

Relaxation Times. From eq 33, we need to evaluate λ_n and ζ_n to obtain τ_n. Putting the total length of the chain as L and taking the continuous chain limit of

$$b \to 0, \qquad N \to \infty, \qquad L = Nb \tag{35}$$

we can express λ_n of eq 25 as

$$\lambda_n = 16\epsilon(n\pi/L)^4 + 4\kappa(n\pi/L)^2 \tag{36}$$

where

$$\epsilon \equiv \lim_{\substack{b\to 0 \\ N\to\infty}} \epsilon_0 b^3 \tag{36a}$$

$$\kappa \equiv \lim_{\substack{b\to 0 \\ N\to\infty}} \kappa_0 b \tag{36b}$$

ϵ is the bending rigidity of the chain and is related to the persistence length, a, by the equation

$$\epsilon = akT \tag{37}$$

Berg gave an equation for obtaining the value of κ as

$$\frac{kT}{(\kappa\epsilon)^{1/2}}\left\{\coth\left(\frac{\kappa L^2}{4\epsilon}\right)^{1/2} - \left(\frac{4\epsilon}{\kappa L^2}\right)^{1/2}\right\} = 1 \tag{38}$$

If eq 38 could be solved for κ, it would be rewritten in a scaled form of

$$\frac{1}{\kappa} = \frac{L^2}{4\epsilon} f\left(\frac{2\epsilon}{LkT}\right) \tag{39}$$

We can easily show that $2\epsilon/LkT = 2a/L$ from eq 37 and $f(x) \sim x^2$ for $x \ll 1$. Therefore, when the contour length,

L, is much longer than the Kuhn statistical segment length, $2a$, κ is expressed approximately as

$$\kappa \sim kT/a \qquad (L \gg 2a) \tag{40}$$

Denoting n at which both terms of eq 36 are the same in magnitude by N_0 and using eq 40, we have

$$N_0 \sim L/2\pi a \tag{41}$$

The ϵ-term is dominant in λ_n of eq 36 for the modes with $n > N_0$ and they are relaxed mainly by the bending rigidity of the chain. On the other hand, the modes with $n < N_0$ relax chiefly with longitudinal tension.

Next, we consider the friction coefficient of the nth mode, ζ_n. Denoting the distance between two beads at intervals of l segments by ρ_l, we have

$$\langle 1/r_{jk} \rangle = \langle 1/\rho_{|j-k|} \rangle \tag{42}$$

because $\langle 1/r_{jk} \rangle$ depends only on $|j - k|$. From eq 13, 16, 28, and 30b, we obtain

$$\zeta_n = \frac{f/b}{1 + \frac{f}{6\pi\eta} \sum_{l=1}^{N-1} \left\langle \frac{1}{\rho_l} \right\rangle \cos\left(\frac{2\pi nl}{N}\right)} \tag{43}$$

Originally, it is only for a pair of beads whose sizes are much smaller than the distance between them that eq 12 can accurately describe the hydrodynamic interaction.[25] Hence, we can safely apply eq 43 only for a chain composed of such beads distinctly separate from each other. On the other hand, any polymer is a continuous chain in the sense that masses distribute continuously along it as long as it is seen with a resolution of monomer unit size. Therefore, in order to obtain an expression of ζ_n that contains not adjustable parameters like those of the RZ model but parameters which can be connected to the molecular structure of the polymer, we must transfer eq 43 to a formula corresponding to the continuous chain. In the following consideration of ζ_n, we will not take into account the apparent longitudinal deformation due to the κ_0-term in eq 6 because it can be assumed negligible for a real wormlike chain.

It is known that stationary transport properties of a continuous chain are well described by a touching-beads model. If the beads of radius $b/2$ are touching each other

$$f = 3\pi\eta b \tag{44}$$

Though eq 12 cannot be used in this case as mentioned above, the form of eq 43 need not be changed if an appropriate expression such as the modified Oseen tensor by Yamakawa and Tanaka[26] is taken for $\langle 1/\rho_l \rangle/(6\pi\eta)$. Substituting eq 44 into eq 43, we obtain

$$\zeta_n = \frac{3\pi\eta}{1 + \frac{b}{2} \sum_{l=1}^{N-1} \left\langle \frac{1}{\rho_l} \right\rangle \cos\left(\frac{2\pi nlb}{L}\right)} \tag{45}$$

Particularly for the translational mode of $n = 0$, we have

$$\zeta_0 = \frac{3\pi\eta}{1 + \frac{b}{2} \sum_{l=1}^{N-1} \left\langle \frac{1}{\rho_l} \right\rangle} \tag{46}$$

Next, we assume that the continuous chain model is described by a wormlike cylinder with radius r_0. After Fujii and Yamakawa,[27] we put $\mathbf{r}$ the vector from a point P_1 on the chain curve to a point P_2 at a distance s along the curve and $\mathbf{r}_0$ the normal radius vector from P_1 to the point on the surface of the cylinder. If we put

$$K(s) \equiv \langle 1/|\mathbf{r} - \mathbf{r}_0| \rangle \tag{47}$$

according to the theory of Fujii and Yamakawa,[27] we have the translational friction coefficient of the circular chain, Ξ_0, as

$$\Xi_0 = \frac{3\pi\eta L}{\int_0^{L/2} K(s)\, ds} \tag{48}$$

The angular brackets in eq 47 mean the average over the vector $\mathbf{r}_0$ and the chain configuration. The relation $K(s) = K(L - s)$ is used in the derivation of eq 48.

Comparing eq 46 with eq 48 and taking account of the fact that ζ_0 is the friction coefficient per unit contour length, we see that the transfer from the discrete model to the continuous one can be carried out by a replacement of

$$1 + \frac{b}{2} \sum_{l=1}^{N-1} \left\langle \frac{1}{\rho_l} \right\rangle \rightarrow \int_0^{L/2} K(s)\, ds \tag{49}$$

Then the extension of the above procedure to ζ_n with $n \neq 0$ can readily be done. Putting $s = lb$ in eq 45, we find ζ_n of the continuous chain

$$\zeta_n = \frac{3\pi\eta}{\int_0^{L/2} K(s) \cos\left(\frac{2\pi ns}{L}\right) ds} \tag{50}$$

In the free-draining case, ζ_n is given from eq 45 by

$$\zeta_n = 3\pi\eta \tag{51}$$

$K(s)$, whose explicit form was given by Fujii and Yamakawa,[27] is a monotonously decreasing function of $|s|$, which has large values at $|s| < r_0$ and decreases very slowly with increasing $|s|$ at $|s| > a$.

It must be remarked here that the demoninator of the right-hand side of eq 50 can be less than 1 for sufficiently large values of n. For such n, ζ_n is larger than that in the free-draining case and can further increase with larger n. The above situation, however, occurs only in the mode with n so large that its "wavelength", L/n, is comparable to or shorter than r_0 and its amplitude is much less than $1/K$. Therefore, such modes offer no serious effect on the evaluation of $S(\mathbf{K},t)$.

The translational diffusion coefficient, D_0, is from eq 48

$$D_0 = \frac{kT}{3\pi\eta L} \int_0^{L/2} K(s)\, ds \tag{52}$$

From eq 33, 36, and 50, the relaxation time τ_n is obtained as

$$\tau_n = (3\pi\eta)/\left[\left\{\int_0^{L/2} K(s) \cos\left(\frac{2\pi ns}{L}\right) ds\right\} \times \{16\epsilon(n\pi/L)^4 + 4\kappa(n\pi/L)^2\}\right] \tag{53}$$

Dynamic Structure Factor. The dynamic structure factor of the initial discrete chain is given by

$$S(\mathbf{K},t) = \alpha_0^2 \sum_{j,k=1}^{N} \langle \exp\{i\mathbf{K}\cdot(\mathbf{r}_j(0) - \mathbf{r}_k(t))\} \rangle \tag{54}$$

where α_0 is the polarizability of the bead. The position of the jth bead is expressed from eq 19 as

$$\mathbf{r}_j(t) = \sum_{n=0}^{N-1} U_{jn}\mathbf{q}_n(t) \tag{55a}$$

Denoting the center of gravity by $\mathbf{r}_g$, we see from eq 20 and 22

$$U_{j0}\mathbf{q}_0 = \frac{1}{N}\sum_{k=1}^{N}\mathbf{r}_k = \mathbf{r}_g \tag{55b}$$

Using eq 55a and 55b and noting that the normal modes including the translational one do not correlate with each other, we find

$$\langle\exp\{i\mathbf{K}\cdot(\mathbf{r}_j(0) - \mathbf{r}_k(t))\}\rangle = \langle\exp[i\mathbf{K}\cdot\{\sum_{n=0}^{N-1}(U_{jn}\mathbf{q}_n(0) - U_{kn}\mathbf{q}_n(t))\}]\rangle = \langle\exp\{i\mathbf{K}\cdot(\mathbf{r}_g(0) - \mathbf{r}_g(t))\}\rangle\langle\exp[i\mathbf{K}\cdot\{\sum_{n=1}^{N-1}(U_{jn}\mathbf{q}_n(0) - U_{kn}\mathbf{q}_n(t))\}]\rangle \tag{56}$$

Solving eq 30 for $n = 0$, we can readily obtain the well-known result

$$\langle\exp\{i\mathbf{K}\cdot(\mathbf{r}_g(0) - \mathbf{r}_g(t))\}\rangle = \exp(-D_0K^2t) \tag{57}$$

Referring to the theory of Uhlenbeck and Ornstein[28] and using eq 20, 31, 32, and 34, we have

$$\langle\exp[i\mathbf{K}\cdot\{\sum_{n=1}^{N-1}(U_{jn}\mathbf{q}_n(0) - U_{kn}\mathbf{q}_n(t))\}]\rangle = \exp\left[-\sum_{n=1}^{N-1}\frac{K^2}{3N}\langle|\mathbf{q}_n|^2\rangle\left\{1 - \cos\left(\frac{2\pi(j-k)}{N}n\right)e^{-t/\tau_n}\right\}\right] \tag{58a}$$

$$= \exp\left[-\sum_{n=1}^{N-1}\frac{2kT\{N - (3/2)\}K^2}{3(N-1)Nb\lambda_n}\left\{1 - \cos\left(\frac{2\pi(j-k)}{N}n\right)e^{-t/\tau_n}\right\}\right] \tag{58b}$$

$$\underset{N\gg1}{\rightarrow} \exp\left[-\sum_{n=1}^{N-1}\frac{2kTK^2}{3L\lambda_n}\left\{1 - \cos\left(\frac{2\pi(j-k)}{N}n\right)e^{-t/\tau_n}\right\}\right] \tag{58}$$

Equation 58a can be derived in the same way as the corresponding formula for RZ chains.[11] In the following, we will consider the case of $N \gg 1$ and use the expression in eq 58. As the exponent in eq 58 is an even function of $(j - k)$, the second factor of eq 56 can be denoted by

$$\langle\exp[i\mathbf{K}\cdot\{\sum_{n=1}^{N-1}(U_{jn}\mathbf{q}_n(0) - U_{kn}\mathbf{q}_n(t))\}]\rangle = c_{|j-k|}(\mathbf{K},t) \tag{59}$$

and we have

$$c_l(\mathbf{K},t) = \exp\left[-\sum_{n=1}^{N-1}\frac{2kTK^2}{3L\lambda_n}\left\{1 - \cos\left(\frac{2\pi l}{N}n\right)e^{-t/\tau_n}\right\}\right] \tag{60}$$

From eq 54 and 56–60, we obtain

$$S(\mathbf{K},t) = \alpha_0^2\exp(-D_0K^2t)\sum_{j,k}c_{|j-k|}(\mathbf{K},t) = N\alpha_0^2\exp(-D_0K^2t)\sum_{l=0}^{N-1}c_l(\mathbf{K},t) \tag{61}$$

We will transform eq 61 into the formula of the continuous chain. Introducing the polarizability per unit length, α, by

$$\alpha \equiv \alpha_0/b \tag{62}$$

we have

$$S(\mathbf{K},t) = L\alpha^2\exp(-D_0K^2t)\sum_{l=0}^{N-1}bc_l(\mathbf{K},t) \tag{63}$$

Putting $s = lb$ and taking the limit of eq 35, we see that $c_l(\mathbf{K},t)$ is transformed into $c(\mathbf{K},s,t)$ as

$$c_l(\mathbf{K},t) \rightarrow c(\mathbf{K},s,t) = \exp\left[-\sum_{n=1}^{\infty}\frac{4kTK^2}{3L\lambda_n}\left\{1 - \cos\left(\frac{2\pi s}{L}n\right)e^{-t/\tau_n}\right\}\right] \tag{64}$$

where use is made of the fact that the two terms for $n = k$ and $n = N - k$ in the exponent of eq 60 have an identical value for each k from 1 to $N - 1$. Taking account of $c(\mathbf{K},L-s,t) = c(\mathbf{K},s,t)$ and making the replacement of

$$\sum_{l=1}^{N-1}b \rightarrow 2\int_0^{L/2}ds$$

in eq 63, we finally get

$$S(\mathbf{K},t) = 2L\alpha^2\exp(-D_0K^2t)\int_0^{L/2}ds\ c(\mathbf{K},s,t) \tag{65}$$

Equation 65 is the dynamic structure factor of the circular Berg chain in which the effect of hydrodynamic interactions is taken into account.

We will introduce some quantities derived from $S(\mathbf{K},t)$. The functions $\Omega(\mathbf{K},t)$ and $D_s(t)$, defined by

$$\Omega(\mathbf{K},t) \equiv -\frac{d}{dt}(\ln S(\mathbf{K},t)) \tag{66}$$

and

$$D_s(t) \equiv \Omega(\mathbf{K},t)/K^2 \tag{67}$$

are respectively the apparent spectral line width and the apparent diffusion coefficient derived from the slope of $S(\mathbf{K},t)$. From eq 64–67, we have

$$D_s(t) = D_0 + \frac{4kT}{3L}\left\{\sum_{n=1}^{\infty}\frac{e^{-t/\tau_n}}{\zeta_n}\int_0^{L/2}ds\ c(\mathbf{K},s,t)\times\cos\left(\frac{2\pi ns}{L}\right)\right\}\Big/\left\{\int_0^{L/2}ds\ c(\mathbf{K},s,t)\right\} \tag{68}$$

The first cumulant, $\Gamma(\mathbf{K})$, of $S(\mathbf{K},t)$ is defined by

$$\Gamma(\mathbf{K}) \equiv \Omega(\mathbf{K},0) \tag{69}$$

and the apparent diffusion coefficient, D_i, obtained from the initial slope of $S(\mathbf{K},t)$ is written as

$$D_i \equiv D_s(0) = \Gamma(\mathbf{K})/K^2 \tag{70}$$

The homodyne photoelectron-pulse correlation function, $C_p(t)$, obtained from DLS measurement is defined by

$$C_p(t) \equiv \langle n(t')n(t'+t)\rangle \tag{71}$$

where $n(t')$ is the number of pulses emitted in a sample time near t'. Assuming the Gaussian nature of the scattered light, which is our case, we have

$$C_p(t) = \langle n\rangle^2(1 + |g^{(1)}(t)|^2) \tag{72}$$

where $g^{(1)}(t)$ is the normalized first-order correlation function of the scattered light field. For later use, we introduce a normalized correlation function, $C(t)$, defined by

$$C(t) \equiv |g^{(1)}(t)|^2 \tag{73}$$

It can readily be shown that $C(t)$ is represented by $S(\mathbf{K},t)$ as

$$C(t) = \left|\frac{S(\mathbf{K},t)}{S(\mathbf{K},0)}\right|^2 \tag{74}$$

Further, we introduce a quantity D_ϵ defined by

$$D_\epsilon \equiv D_s(t_\epsilon) \tag{75}$$

where t_ϵ is the time at which $C(t) = 0.01$. The static structure factor, $P(\mathbf{K})$, is given by

$$P(\mathbf{K}) = \frac{S(\mathbf{K},0)}{S(\mathbf{0},0)} = \frac{2}{L}\int_0^{L/2} ds\, c(\mathbf{K},s,0) \qquad (76)$$

III. Results of the Numerical Calculation and Discussion

Due to the complex form of the function $K(s)$, it is difficult to analytically express $c(\mathbf{K},s,t)$. Thus, the dynamic structure factor in eq 65 and the related quantities introduced in section II were evaluated numerically for parameter values corresponding to native DNA. The minimal parameters that characterize the continuous Berg model are the contour length, L, the hydrodynamic diameter, d, and the bending rigidity, ϵ. The value of d was fixed to the mean accepted value of 2.5 nm. According to eq 37, the persistence length, a, in place of ϵ was used. We assumed water as the solvent, whose condition is specified by temperature, T, and viscosity, η. The temperature was fixed to 25 °C except for the calculation of temperature dependence.

The process of the numerical calculation is as follows. κ is obtained by solving eq 38 for given values of L, T, and a. λ_n and ζ_n are calculated from eq 36 and 50, respectively. The value of $K(s)$ necessary for the evaluation of ζ_n is obtained by using eq 10–12 of Fujii and Yamakawa.[27] Then $c(\mathbf{K},s,t)$ is evaluated by eq 64 for the above values of λ_n and ζ_n. Finally, the substitution of $c(\mathbf{K},s,t)$ into eq 65, 68, and 71 yields the respective quantities. The upper limit of n of the series in the expression of $c(\mathbf{K},s,t)$ (eq 64), which is denoted by N_m, was taken large enough for the contribution from the terms with $n > N_m$ to be negligible.

A single-exponential function of the form

$$f_{se}(t) = A \exp(-2D_a K^2 t) + B \qquad (77)$$

was fitted to the normalized homodyne correlation function, $C(t)$, in the time range of $0 < t < t_c$. The fitted value of D_a, which has the meaning of apparent diffusion coefficient, is used to characterize the dependence of $C(t)$ on K. The fitting was made for both cases in which B is varied and fixed to zero. We will denote the values of D_a for the former and latter cases by D_{a1} and D_{a0}, respectively. Defining δ by A and B obtained from the former analysis as

$$\delta \equiv B/(A + B) \qquad (78)$$

we can use it as the quantity that measures the non-single-exponentiality of $C(t)$.

In order to compare with the continuous Berg chain, numerical calculations were also made on a circular, flexible bead chain. It is a hypothetical mathematical model and characterized as follows:

(1) It is made up of N beads and N springs; accordingly it has $3N - 3$ internal modes.

(2) λ_n is taken as

$$\lambda_n = (4\kappa/b^2) \sin^2 (n\pi/N) \qquad (79)$$

That is, it has no term of bending elasticity corresponding to the first term of eq 25. κ is assumed to be given also by eq 38 for the corresponding Berg chain.

(3) The value of ζ_n is taken to be the same as eq 50.

We will denote continuous semiflexible and discrete flexible chains as CS and DF chains, respectively, in the following. Both λ_n of eq 25 and 79 coincide with each other in the limit of $n/N \to 0$. Hence, the DF model gives the same $S(\mathbf{K},t)$ as the CS model in the small-K region where lower modes are dominant in $S(\mathbf{K},t)$. By assuming the same hydrodynamic interaction, only the effect of the differences in chain continuity and bending elasticity between the two models will be made clear, especially in the large-K range. This is the reason why an artificial DF model rather than the RZ model was chosen for comparison.

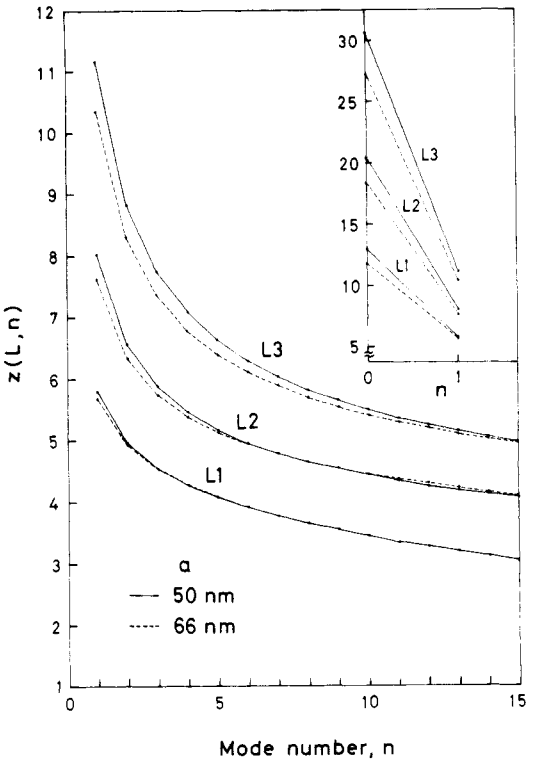

Figure 1. Hydrodynamic interaction factor, $z(L,n)$, for CS chains with different contour lengths: $L_1 = 2.24$ μm, $L_2 = 6.60$ μm, and $L_3 = 16.6$ μm. Persistence length, a: solid lines, 50 nm; broken lines, 66 nm.

Numerical calculations were all made with double-precision numbers.

Hydrodynamic Interaction Factor. The hydrodynamic interaction factor, $z(L,n)$, defined by

$$z(L,n) \equiv \int_0^{L/2} K(s) \cos\left(\frac{2\pi n}{L}s\right) ds \qquad (80)$$

is plotted in Figure 1 for CS chains with different contour lengths, $L_1 = 2.24$ μm, $L_2 = 6.60$ μm, and $L_3 = 16.6$ μm. As seen from eq 50 and 51, $z(L,n)$ is the ratio of friction coefficients of the nth normal modes for the model without and with hydrodynamic interaction. L_1 and L_3 correspond to ColEl and λ-DNA, respectively. $z(L,n)$ falls drastically with the change of n from 0 to 1 and decreases slowly with n larger than 1. When chains of different persistence lengths are compared, $z(L,n)$ of the chain with $a = 66$ nm is larger at small n than that with $a = 50$ nm. But for n exceeding a value determined by L, the relation of magnitude is reversed. The above reversal occurs at $n = 2.5$, 7.4, and 18.7 for L_1, L_2, and L_3, respectively. However, the relative differences of $z(L,n)$ for two values of a decrease rapidly with n and become less than 1% at n larger than 1, 4, and 12 for L_1, L_2, and L_3, respectively. That is, the dependence of ζ_n on persistence length rapidly becomes small with increasing n.

It can also be shown from the reuslts of numerical calculations that $z(L,n)$ for the internal modes with $n \neq 0$ is approximately scaled by n/L; i.e., it can be expressed as

$$z(L,n) \sim z(n/L) \qquad (81)$$

For example, the relative difference between $z(L_1,n_1)$ and $z(L_3, L_3 n_1/L_1)$, the latter of which is estimated by an interpolation of the $z(L_3,n)$ curve, is 9% of $z(L_1,n_1)$ at $n_1 = 1$. It decreases with increasing n_1 to become less than 1%

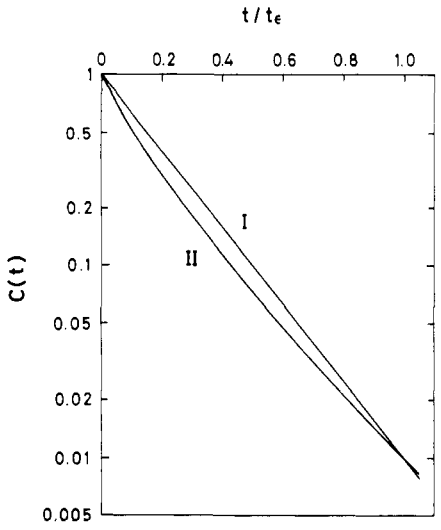

Figure 2. Typical examples of the calculated correlation functions, $C(t)$, for a CS chain: L = 6.60 μm, A = 66 nm, and T = 25.0 °C. Values of K^2 (m^{-2}): I, 7.0 × 10^{12}; II, 7.0 × 10^{14}. t_ϵ is the time at which $C(t)$ = 0.01.

at n_1 greater than 5. The scaling property of $z(L,n)$ results from the characteristic form of the function $K(s)$ described in section II. The fact that $z(L,n)$ of the higher modes is scaled with better accuracy means that the effect of the hydrodynamic interactions on the local motion of a chain is independent of the total chain size.

Shape of Correlation Functions. Two typical examples of the calculated correlation functions, $C(t)$, for a CS chain with $L = L_2$ and a = 66 nm are shown in Figure 2. The chain length corresponds to $50l_K$, where $l_K = 2a$ denotes the Kuhn statistical segment length. Disregarding the excluded volume effect, we obtain 265 nm for the root-mean-square radius, R, of this chain from the formula

$$R = \left[aL\left\{\frac{1}{6} - \frac{a}{2L} + \frac{a^2}{L^2} - \frac{a^3}{L^3}(1 - e^{-L/a})\right\}\right]^{1/2} \quad (82)$$

Substitution of the above value of R into $K^2R^2 = 2$ yields 2.84 × 10^{13} m^{-2} for the K^2 value at which the contribution of the lowest internal mode begins to be significant. Curve I in the figure is an example of $C(t)$ at small angles (K^2 = 7.0 × 10^{12} m^{-2}), and the $C(t)$ is a single-exponential function. Curve II (K^2 = 7.0 × 10^{14} m^{-2}) is typical of the correlation functions at K^2 where the intramolecular motion is dominant, and the $C(t)$ clearly shows a non-single-exponential form. Thus, generally, $C(t)$ or $S(\mathbf{K},t)$ is not a single-exponential function and its functional form cannot be characterized only by its first cumulant.

In Figure 3 is shown the K^2 dependence of δ defined by eq 78. The filled circle on each curve corresponds to the K^2 value which satisfies the relation of $K^2R^2 = 2$ noted above. δ increases with K^2 and reaches a nearly constant value in the K^2 region where intramolecular motion dominates $C(t)$. The value of δ in the saturation region is about 2% and increases slightly with L.

In order to see more precisely the deviation of correlation functions from a single-exponential form, $D_s(t)$, defined by eq 68, is plotted in Figure 4. The abscissa is the logarithm of the delay time scaled by t_ϵ. The values of D_s on the intersection of each curve with the left and the right axes of the ordinate are D_i and D_ϵ, respectively. At K^2 = 7.0 × 10^{14} m^{-2} in the saturation region of Figure 3, we have

$$D_i/D_\epsilon = 2.16$$
$$D_i/D_{s0} = 1.39 \quad (83)$$

That is, the apparent diffusion coefficient obtained from

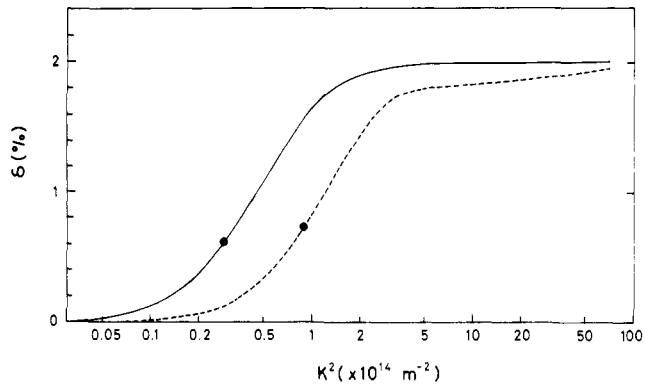

Figure 3. δ vs. K^2 for two CS chains with different contour lengths: solid line, L = 6.60 μm; broken line, L = 2.24 μm. a = 66 nm and T = 25.0 °C are assumed. See the text for explanation of the filled circles on the curves.

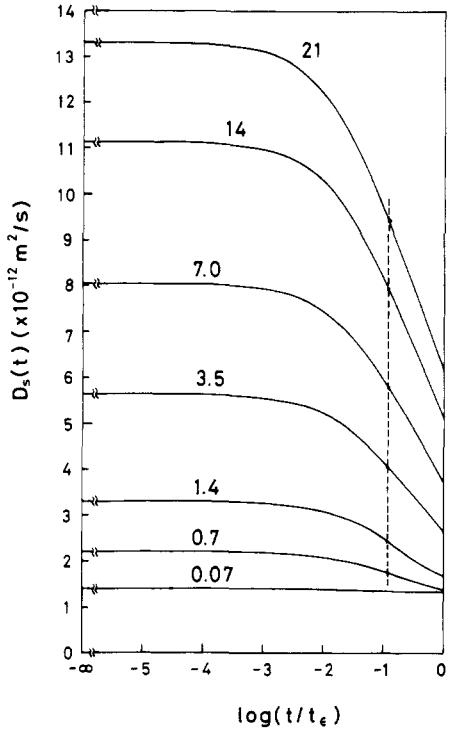

Figure 4. $D_s(t)$ vs. normalized delay time for a CS chain: L = 6.60 μm, a = 66 nm, and T = 25.0 °C. The number at each curve indicates the K^2 value in units of 10^{14} m^{-2}. t_ϵ is the time at which $C(t)$ = 0.01.

the first cumulant has more than twice the value of D_ϵ and is 39% larger than D_{s0}, which is given by a single-exponential approximation. As seen from the figure, $D_s(t)$ begins to decrease from a fairly small value of t. For example, a determination of the value of D_i within the accuracy of 5% requires a measurement of the slope of $C(t)$ at $(t/t_\epsilon) \sim 5.5 \times 10^{-3}$. Thus, in order to compare quantitatively the initial slope of a $C(t)$ with the first-cumulant theory, measurement must be made of the $C(t)$ with a short delay time of the order of $(t/t_\epsilon) \sim 10^{-3}$. The broken line in the figure is generated by connecting the point on each curve at which $D_s(t)$ takes the same value as the D_{s0} of the corresponding $C(t)$. Interestingly, the scaled delay time at which $D_s(t) = D_{s0}$ is nearly independent of K^2 and given by

$$t/t_\epsilon \sim 0.12 \quad (84)$$

K Dependence of Apparent Diffusion Coefficients and Comparison of CS and DF Chains. In Figure 5 are displayed K^2 dependences of D_i, D_{s1}, D_{s0}, and D_ϵ. The figure shows that D_{s0} and D_{s1} are near the mean value of

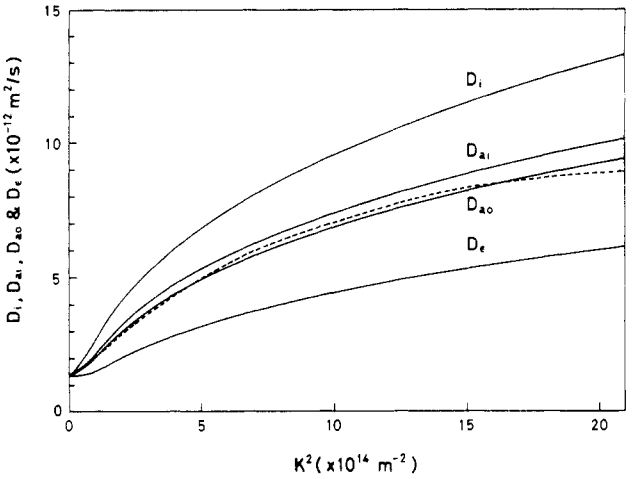

Figure 5. Dependences of the apparent diffusion coefficients (D_i, D_{a1}, D_{a0}, and D_ϵ) on K^2: L = 6.60 μm, a = 66 nm, and T = 25.0 °C. The broken line represents the data for ϕ_{29} DNA by Thomas et al.[13]

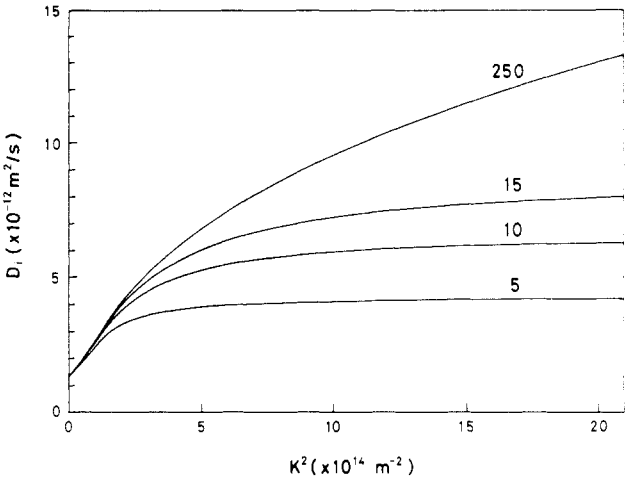

Figure 6. D_i vs. K^2 for a CS chain: L = 6.60 μm, a = 66 nm, and T = 25.0 °C. The number at each curve indicates the value of N_m. In this K^2 range, the curve of N_m = 250 can in practice be assumed to be identical with that of $N_m = \infty$.

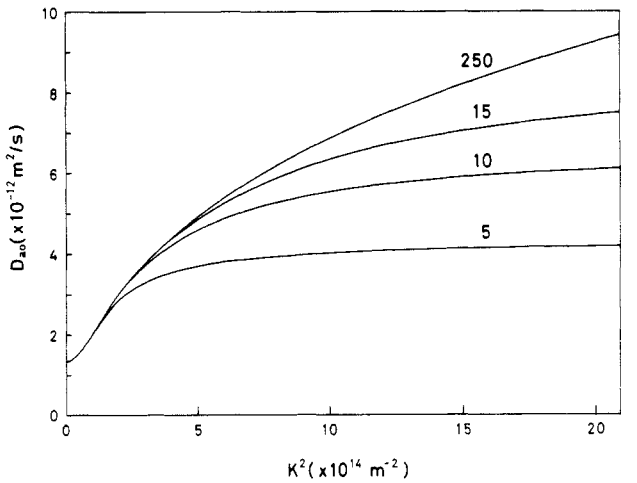

Figure 7. D_{a0} vs. K^2 for a CS chain. Parameters are the same as in Figure 6.

D_i and D_ϵ. We can recognize that, in order to examine DLS data quantitatively, we must specify the range of delay time of the data used for the analysis. The broken line corresponds to the data of ϕ_{29} DNA (L = 5.9 μm) measured by Thomas et al.[13] Their data show a K^2 dependence very similar to those of D_{a0} and D_{a1} from our theory. If any difference exists at all, it may be that their data seem to show a tendency to saturate at K^2 larger than 15×10^{14} m^{-2}. On the basis of this fact, they assert the applicability of the RZ model to native DNA. As the form and length of our model chain and their DNA molecules are different, it may be meaningless to compare our theory with their experiment in detail for testing the accuracy of our theoretical prediction. If we assume the effect of the above differences to be negligible and the deviation of the experimental curve from the theoretical one at large K^2 is a true deviation exceeding experimental error, the discrepancy might be due to some incompleteness of our model, which is discussed in section IV.

Recently, Wilcoxon and Schurr[29] gave an exact expression of $\Gamma(\mathbf{K})$ for a thin rod and predicted that $\mathbf{D}_i$ derived from $\Gamma(\mathbf{K})$ reaches a limiting plateau value at sufficiently large K. If we assume that a DNA molecule can be modeled by a sequence of rigid rods with a length of the order of its persistence length, it is inferred from their results that D_i of DNA also reaches a saturated value at large K. It is an interesting problem to be solved how the K dependence of D_i for a real DNA molecule with a finite bending rigidity differs from that of a chain composed of a sequence of rigid rods in the very large K region. Wilcoxon and Schurr found also that the approach of D_i of a rigid rod to its plateau value with increasing K^2 was extremely slow. Judging from this result and reported data on DNA,[13] it seems very difficult to estimate the accurate plateau value of D_i of DNA only from DLS data in the presently available range of K^2, even if D_i of DNA truly saturates at sufficiently large K^2. In order to predict the true behavior of apparent diffusion coefficients of DNA at very large K^2, it may be necessary to give an expression of the dynamic structure factor for a model refined by including the effect of chain stiffness in a more complete form.

K^2 dependences of D_i and D_{a0} are shown in Figures 6 and 7 respectively for various values of N_m taken in the evaluation of $c(\mathbf{K},s,t)$ in eq 64. The value of N_0 of this chain is given from eq 41 as

$$N_0 \sim 16 \tag{85}$$

Thus, the part bounded by the curves of N_m = 15 and 250 can approximately be assumed to be the contribution of the modes which are relaxed by the bending elasticity of the chain. Comparison of both leads to the fact that D_i has a larger relative contribution from higher modes than D_{a0} and exhibits a prominent effect of bending elasticity even at low values of K^2. For example, at $K^2 = K_0^2 = 7.0 \times 10^{14}$ m^{-2}, which is the maximum value of K^2 available using the He–Ne laser, the portion of the contribution of the modes with $n > 15$ is 4% in D_{a0} and 17% in D_i. This portion increases with K^2 for both D_i and D_{a0} and reaches as much as 39% for D_i at $K^2 = 20 \times 10^{14}$ m^{-2}.

D_i of DF chains with different bead numbers, N, are plotted in Figure 8 to show the effect of bead number. Compared with CS chains, the notable characteristic of a DF chain is that D_i reaches a plateau value for K^2 large enough for each bead to be resolved as described by Lin and Schurr.[11] When N is made small, the saturated value of D_i also becomes smaller, and saturation occurs at smaller K^2. If K^2 is so large that the inequality

$$2kTK^2/3L\lambda_n \gg 1 \tag{86}$$

holds for all n from 1 to $N - 1$ in eq 60, only c_l with l = 0 has a significant value. In the range of time, t, short enough to allow for all nonzero n the expansion of

$$\exp(-t/\tau_n) \sim 1 - t/\tau_n \tag{87}$$

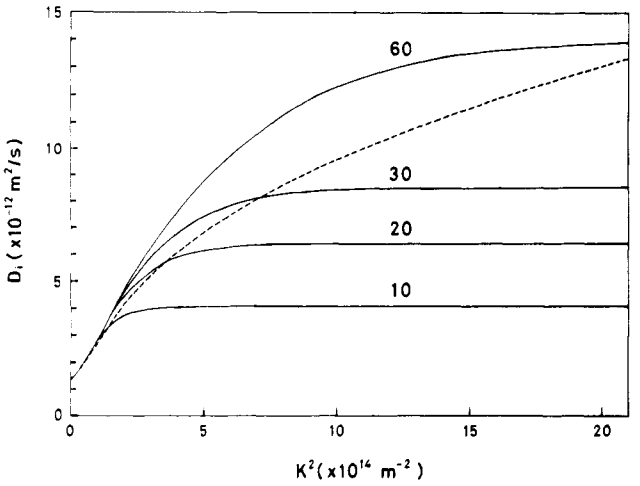

Figure 8. D_i vs. K^2 for DF chains with different bead numbers, N. The bead number is indicated at each curve. The broken line is the D_i curve with $N_m = 250$ for the same chain as in Figure 6. Other parameters of these DF chains are taken so that their $C(t)$ and that of the above CS chain may coincide with one another in the small-K region (see text).

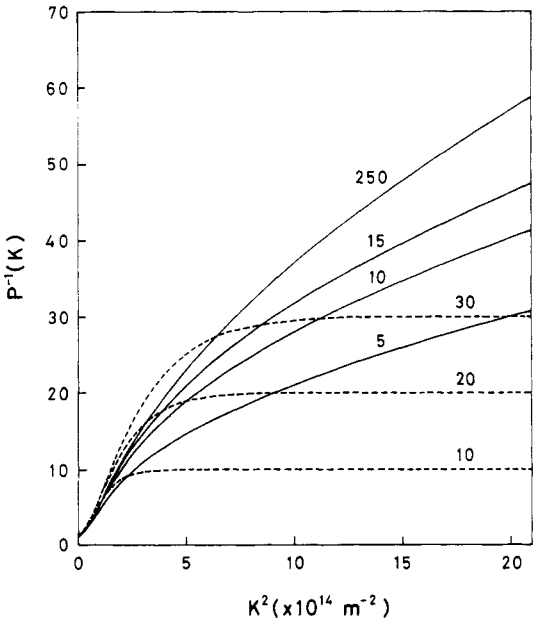

Figure 9. Dependence of the reciprocal static structure factor, $P^{-1}(\mathbf{K})$, on K^2 for CS (solid lines) and DF (broken lines) chains. Parameters for CS and DF chains are the same as in Figures 6 and 8, respectively.

$S(\mathbf{K},t)$, from eq 61, has approximately a single-exponential form of

$$S(\mathbf{K},t) \sim N\alpha_0^2 \exp\left\{-\left(D_0 + \sum_{n=1}^{N-1} \frac{2kT}{3L\zeta_n}\right)K^2 t\right\} \quad (88)$$

Thus, the saturated value of D_i is given by

$$D_i \sim D_0 + \sum_{n=1}^{N-1} \frac{2kT}{3L\zeta_n} \quad (89)$$

Equation 88 means that each bead is seen to be making a free and independent diffusive motion in the K^2 region. Though it is not shown in the figure, D_{a0} and D_{a1} also exhibit similar dependences on K^2, which is a common property of the discrete spring–bead models.

Reciprocal static structure factors, $P^{-1}(\mathbf{K})$, for CS and DF chains are displayed in Figure 9. $P^{-1}(\mathbf{K})$ of the CS chain increases with K^2 even for smaller values of N_m, while

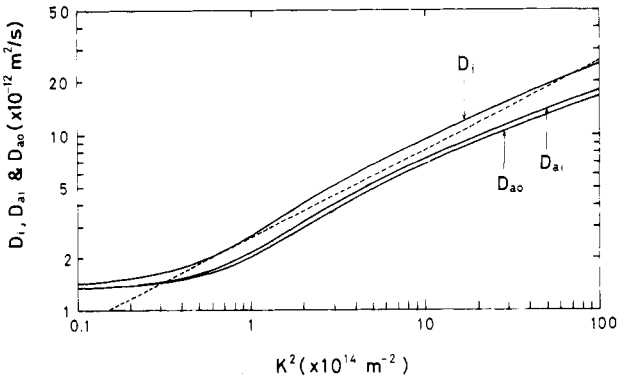

Figure 10. log–log plots of the apparent diffusion coefficients (D_i, D_{a1}, and D_{a0}) vs. K^2 for a CS chain. Parameters are the same as in Figure 5. The broken line is a straight line with a slope of 1/2 corresponding to the relation $\Gamma_s \propto K^3$.

that of the DF chain reaches a constant at large value of K^2 as in the case of the apparent diffusion coefficient. The portion of the contribution from the modes of $n > 15$ in the CS chain increases with K^2 and accounts for 12% of the entire contribution at $K^2 = 7.0 \times 10^{14}$ m^{-2}. The saturated value of $P^{-1}(\mathbf{K})$ of a DF chain is equal to its number of beads, N, which also means that each bead is seen to be independent in the large-K^2 region.

Sadron[30] and Ptitsyn and Fedorov[31] found that $P^{-1}(\mathbf{K})$ of native DNA at large K^2 is well described by a linear function of K as

$$P^{-1}(\mathbf{K}) = A_0 K + B_0 \quad (90)$$

where A_0 and B_0 are respectively a positive and negative constant determined from molecular parameters of the DNA. By plotting $P^{-1}(\mathbf{K})$ of the CS chain with $N_m = 250$ in Figure 9 against K, it is found that $P^{-1}(\mathbf{K})$ lies on a straight line very well at $K > 1.8 \times 10^7$ m^{-1} or $K^2 > 3.2 \times 10^{14}$ m^{-2} (figure not shown). The line extrapolated to $K = 0$ gives a negative intersection with the ordinate axis, which agrees with the results of Sadron.[30] Comparison of $P^{-1}(\mathbf{K})$ derived from our theory with that from the theory of wormlike chains[32,33] would serve as a quantitative test of our theory, which will be made elsewhere.

To see the exponent in the K dependences of apparent diffusion coefficients which have the dimension of spectral line width divided by K^2, the log–log plot of the curves in Figure 5 is made in Figure 10. The theoretical curve of the CS chain shows a feature clearly different from the K^3 dependence of spectral line width predicted for the RZ model.[2] All curves of D_i, D_{a0}, and D_{a1} are convexly shaped at $K^2 > 1.4 \times 10^{14}$ m^{-2} where the internal motion dominates $C(t)$. If we put

$$D_i,\ D_{a0},\ \text{and}\ D_{a1} \propto K^{\gamma-2} \quad (91)$$

we have, in the range of $K^2 = (4\text{–}10) \times 10^{14}$ m^{-2}, $\gamma \sim 3$, which is equal to that of RZ chains.[2] But at K^2 smaller than the above, γ is significantly larger than 3 and takes the maximum of 3.2 near $K^2 \sim 1.4 \times 10^{14}$ m^{-2}. On the other hand, at $K^2 > 10 \times 10^{14}$ m^{-2}, γ is smaller than 3 and decreases with increasing K^2, which agrees with the data of Thomas et al.[13] However, it is found that γ does not reach the plateau value, 2, for RZ chains in the range of $K^2 < 10^{16}$ m^{-2} where the calculation was made, which is opposed to the prediction by Schurr et al.[11,17]

Effect of Chain Stiffness, Chain Length, and Temperature. D_{a1} for four values of persistence length is shown in Figure 11 to see the effect of chain stiffness. The shorter the persistence length, the larger is the translational diffusion coefficient because the chain becomes more

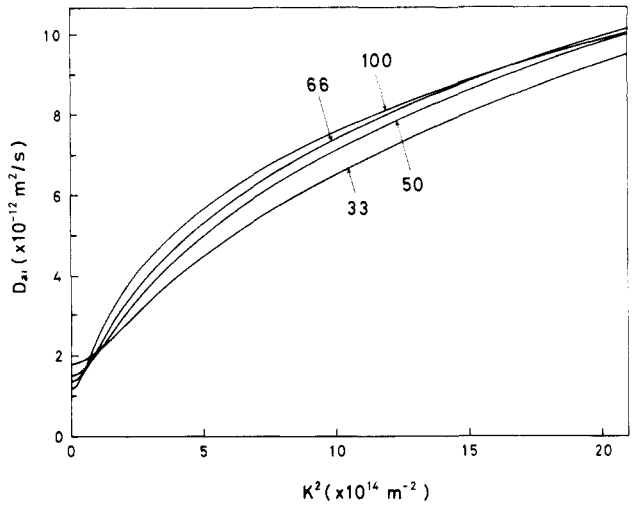

Figure 11. Dependence of D_{a1} on K^2 for CS chains with different persistence lengths, a: L = 6.60 μm and T = 25.0 °C. The numbers beside the curves indicate the value of a (nm).

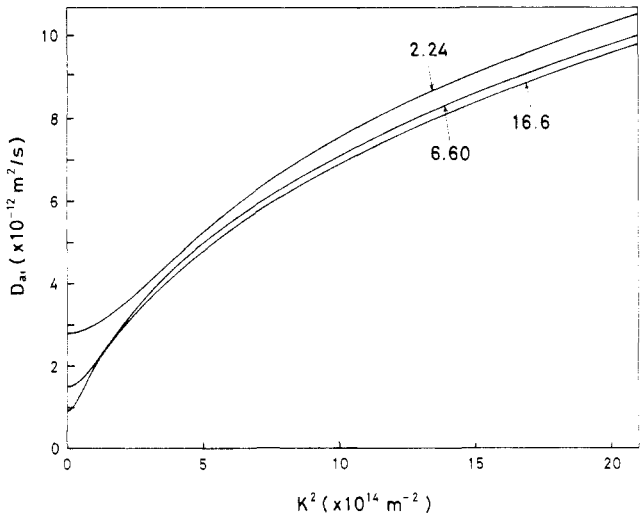

Figure 12. Dependence of D_{a1} on K^2 for CS chains with different contour lengths, L: a = 50 nm (i.e., l_K = 0.1 μm) and T = 25.0 °C. The numbers beside the curves indicate the value of L (μm).

compact. In the large-K^2 region, the stiffer chain gives the larger D_{a1} except for the case of a = 100 nm at $K^2 > 16 \times 10^{14}$ m^{-2}. However, the dependence of D_{a1} on a is relatively small at large K^2. For example, D_{a1} decreases only by 18% at $K^2 = 7.0 \times 10^{14}$ m^{-2} when the persistence length is changed by a factor of 3 from 100 to 33 nm. Further, the values of D_{a1} for three chains with longer persistence lengths differ by less than 2.5% at $K^2 > 15 \times 10^{14}$ m^{-2}. Therefore, it is necessary to take account of the relative insensitivity of the apparent diffusion coefficient to persistence length when discussing the chain stiffness with DLS data.

Chains having different contour lengths and the same stiffness are compared in Figure 12. The Kuhn statistical length, l_K, of the chains is 0.1 μm. Compared in the K^2 region where internal motion dominates $C(t)$, the difference between the curves of $L = L_2$ and L_3 is much smaller than the difference between those of $L = L_1$ and $L = L_2$ or L_3. This means that, though the effect of a finite contour length on the DLS property is almost negligible for the chain with $L = L_2$ ($66l_K$) or L_3 ($166l_K$), it is significant for the chain with $L = L_1$ ($22l_K$). It can also be seen from the figure that the effect of the contour length appears most notably in the magnitude of the translational diffusion coefficient given in the limit of $K^2 \to 0$.

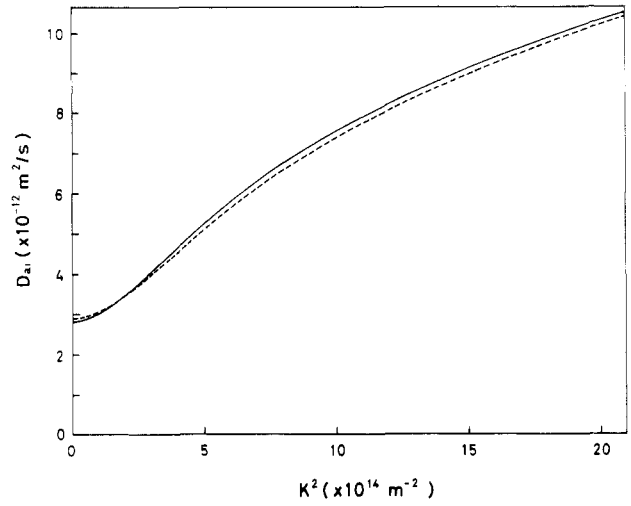

Figure 13. D_{a1} vs. K^2 for a CS chain at different temperatures: solid line, T = 25 °C and a = 50 nm; broken line, T = 55 °C and a = 45.4 nm. L = 2.24 μm is assumed.

Finally, the temperature effect on D_{a1} is shown in Figure 13. The chain with a = 50 nm at 25 °C is compared with the same chain having a = 45.4 nm at 55 °C in accordance with eq 37. D_{a1} for 55 °C in the figure is reduced to the condition of T = 25 °C by multiplying D_{a1} derived from $C(t)$ at 55 °C by the temperature viscosity factor of $298.15 \times 5.072/(328.15 \times 8.949) = 0.5150$. The figure shows that D_{a1} does not scale with η/T. However, the difference between the two curves is very small. Though the difference in persistence length is about 10%, the difference of D_{a1} amounts to only 3.1% even for the translational diffusion coefficient at $K \to 0$ for which the difference is largest.

IV. Conclusion and Comments

In this paper, Berg's theory of circular semiflexible chains was extended by including the hydrodynamic interaction effect, and an expression of $S(\mathbf{K},t)$ was given. It was shown by numerical calculation that this theory made it possible to evaluate, at least semiquantitatively, the DLS properties of semiflexible chains using molecular parameters rather than free ones. However, several crucial assumptions and approximations are made in the present theory. Some refinement seems necessary for applying the theory to the quantitative analyses of more precise data. Therefore, it is instructive to list those assumptions and to discuss their possible effects.

(1) The Berg model, whose potential energy is given by eq 6, is not a model for wormlike chains. The Berg chain is highly flexible in the direction of the chain axis[34] unlike real wormlike molecules. Decoupling into the normal modes is made possible by assuming a special form of internal stress originating in the potential energy. Further, it is assumed that, in the original discrete model, the thermal energy equivalent to that of $2N$ degrees of freedom is equally partitioned among $3N$ independent normal modes. Though it seems hard to evaluate quantitatively the difference in the motions of the model chain and the real wormlike one, they will certainly differ. This difference in motion between the two chains might cause a substantial difference between their dynamic structure factors, especially at large K where the local dynamic property of a chain is more significant for determining its dynamic structure factor.

For a model closer to real wormlike chains, we have an array of mechanical springs with a bending elasticity as described earlier.[35] Though the author gave the Langevin

equation of motion for such chains, it seems difficult to obtain an analytical solution because of its nonlinear form.

(2) The Oseen tensor is preaveraged in the evaluation of intramolecular hydrodynamic interaction.

According to Benmouna and Akcasu[9] and Burchard et al.,[36] the first cumulant of a linear flexible chain estimated using a preaveraged Oseen tensor can be a maximum of 15% smaller than the case without preaveraging. Therefore, it is naturally expected that preaveraging may cause an effect to the above extent also in our case.

(3) Several approximations are made in the evaluation of the function $K(s)$ necessary for the calculation of ζ_n. Especially, as $K(s)$ is large in the neighborhood of $s = 0$, the accuracy of its value near $s = 0$ can have a significant effect on the accuracy of ζ_n.

(4) The effect of torsional elasticity is not taken into account. It was indicated from the measurement of fluorescence anisotropy decay of dyes intercalated into native DNA[37-39] that the torsional rigidity of native DNA has the same order of magnitude as the bending rigidity. Hence, the coupling of bending and torsional motions is readily anticipated.[16]

(5) The excluded volume effect is not taken into consideration. The apparent persistence length is considered to decrease as the spatial resolution becomes higher with increasing K^2, because the excluded volume effect is more significant for the larger-scale property of a chain molecule. Accordingly, if the measured D_{a1} vs. K^2 curve in Figure 5 apparently exhibits a saturation tendency, it can also be interpreted to mean that the curve approaches the theoretical curve with a lower value of a at higher K^2. Qualitatively speaking, the behavior of the curve can be a manifestation of the excluded volume effect.

Last, we will note on the applicability of our theory to linear chains. The internal motion of a chain molecule whose contour length is much longer than its persistence length, is considered to hardly depend on its form: circular or linear. Therefore, our expression of dynamic structure factor for circular chains is expected to be a good approximation of that for linear chains except in the low-K region where the effect of translational motion is dominant. The results shown in Figures 5 and 12 actually suggest that the above inference is true. Extension of the present theory for applying it to linear chains is now in progress.

Acknowledgment. The author is grateful to Professor A. Wada for his encouragement throughout this work. The author also thanks Dr. M. Schmidt and Professor W. H. Stockmayer, who kindly sent him a preprint of their paper.

References and Notes

(1) de Gennes, P.-G. *Physics (Long Island City, N.Y.)* **1967**, *3*, 37.
(2) Dubois-Violette, E.; de Gennes, P.-G. *Physics (Long Island City, N.Y.)* **1967**, *3*, 181.
(3) de Gennes, P.-G. *Nature (London)* **1979**, *282*, 367.
(4) Zimm, B. H. *J. Chem. Phys.* **1956**, *24*, 269.
(5) Pecora, R. *J. Chem. Phys.* **1968**, *49*, 1032.
(6) Jolly, D.; Eisenberg, H. *Biopolymers* **1976**, *15*, 61.
(7) Chen, F. C.; Yeh, A.; Chu, B. *J. Chem. Phys.* **1977**, *66*, 1290.
(8) Akcasu, A. Z.; Gurol, H. *J. Polym. Sci., Polym. Phys. Ed.* **1976**, *14*, 1.
(9) Benmouna, M.; Akcasu, A. Z. *Macromolecules* **1980**, *13*, 409.
(10) Benmouna, M.; Akcasu, A. Z.; Daoud, M. *Macromolecules* **1980**, *13*, 1703.
(11) Lin, S.-C.; Schurr, J. M. *Biopolymers* **1978**, *17*, 425.
(12) Kratky, O.; Porod, G. *Recl. Trav. Chim. Pays-Bas* **1949**, *68*, 1106.
(13) Thomas, J. C.; Allison, S. A.; Schurr, J. M.; Holder, R. D. *Biopolymers* **1980**, *19*, 1451.
(14) Parthasarathy, N.; Schmitz, K. *Biopolymers* **1980**, *19*, 1655.
(15) Lin, S.-C.; Thomas, J. C.; Allison, S. A.; Schurr, J. M. *Biopolymers* **1981**, *20*, 209.
(16) Wilcoxon, J.; Schurr, J. M. *Biopolymers* **1983**, *22*, 2273.
(17) Schurr, J. M. *Biopolymers* **1983**, *22*, 2207.
(18) Harris, R. A.; Hearst, J. E. *J. Chem. Phys.* **1966**, *44*, 2595.
(19) Hearst, J. E.; Beals, E.; Harris, R. A. *J. Chem. Phys.* **1968**, *48*, 5371.
(20) Berg, O. G. *Biopolymers* **1979**, *18*, 2861.
(21) Peterlin, A. *J. Polym. Sci.* **1953**, *10*, 425.
(22) Saito, N.; Takahashi, K.; Yunoki, Y. *J. Phys. Soc. Jpn.* **1967**, *22*, 219.
(23) Maeda, T.; Fujime, S. *Macromolecules* **1981**, *14*, 809.
(24) Schmidt, M.; Stockmayer, W. H. *Macromolecules* **1984**, *17*, 514.
(25) Yamakawa, H. "Modern Theory of Polymer Solutions"; Harper and Row: New York, 1971.
(26) Yamakawa, H.; Tanaka, G. *J. Chem. Phys.* **1972**, *57*, 1537.
(27) Fujii, M.; Yamakawa, H. *Macromolecules* **1975**, *8*, 792.
(28) Uhlenbeck, G. E.; Ornstein, L. S. *Phys. Rev.* **1930**, *36*, 823.
(29) Wilcoxon, J.; Schurr, J. M. *Biopolymers* **1983**, *22*, 849.
(30) Sadron, Ch. *J. Chim. Phys.* **1961**, *58*, 877.
(31) Ptitsyn, O. B.; Fedorov, B. A. *Biofizika* **1963**, *8*, 659.
(32) Yamakawa, H.; Fujii, M. *Macromolecules* **1974**, *7*, 649.
(33) des Cloizeaux, J. *Macromolecules* **1973**, *6*, 403.
(34) Simon, E. *J. Chem. Phys.* **1970**, *52*, 3879.
(35) Soda, K. *J. Phys. Soc. Jpn.* **1973**, *35*, 866.
(36) Burchard, W.; Schmidt, M.; Stockmayer, W. H. *Macromolecules* **1980**, *13*, 580.
(37) Wahl, Ph.; Paoletti, J.; Le Peeq, J.-B. *Proc. Natl. Acad. Sci. U.S.A.* **1970**, *65*, 417.
(38) Thomas, J. C.; Allison, S. A.; Appellof, C. J.; Schurr, J. M. *Biophys. Chem.* **1980**, *12*, 177.
(39) Miller, D. P.; Robbins, R. J.; Zewail, A. H. *J. Chem. Phys.* **1982**, *76*, 2080.